Chapter 6

Mixed Natural Element Method in Linear Elasticity

In this Chapter, we pursue a mixed displacement-pressure formulation for the natural element method in linear elastostatics. In the following section, a brief background on mixed formulations is presented. Then, the NEM displacement and pressure interpolants are presented, followed by the governing equations for the boundary value problem of linear elastostatics (incompressible and compressible cases). Finally, applications of the mixed natural element method for the cantilever beam in bending, and for the plate with a circular hole under uniaxial tension are presented.

6.1 Background

Variational formulations that are based on Hellinger-Reissner principle and the Hu-Washizu principle (Washizu, 1982) are well-established and widely-used in finite elements. The term mixed methods refers to finite element methods in which two different fields (for eg., displacement and stress or displacement and strain) are approximated as primary variables; in linear elastostatics, mixed methods assume a particular form of the Hellinger-Reissner variational principle. There are significant advantages that accrue when one departs from a displacement-based Galerkin method to one involving a two-field or three-field variational principle. The motivation and interest in mixed finite element methods stems from quite a few factors: first, in structural analysis the stress tensor $\boldsymbol{\sigma}$ is very often the key field variable of interest, which can be directly obtained from the solution of a mixed analysis; mixed formulations impose less stringent continuity requirements on the trial and test function spaces, and as a result C^0 trial functions suffice for fourth-order problems that are posed in a mixed variational framework; mixed methods facilitate the representation of smoothly varying stress (pressure) fields by using C^0 interpolation for the stresses (pressure); and lastly, the judicious choice of functions spaces for the primary fields in mixed formulations permits robust and accurate solutions of boundary value problems in limiting cases, such as near incompressibility (Poisson locking) in linear elastostatics when the Poisson's ratio $\nu \to 0.5$, and membrane and shear locking in thin beam and plate problems as the thickness $t \to 0$. A caveat to the above optimism is that the choice of function spaces for the primary fields in mixed methods can not be arbitrary; the accuracy and convergence of the method relies on how well the discrete finite-dimensional subspaces approximate their continuous counterparts, and more importantly, if the discrete function spaces satisfy the Ladyzhenskaya-Babuška-Brezzi (LBB) or inf-sup stability condition (Ladyzhenskaya, 1969; Babuška, 1971; Brezzi, 1974).

Locking in finite elements has primarily been approached using modified variational principles, such as assumed strain methods (Simo and Hughes, 1986), assumed stress methods (Pian and Sumihara, 1984), and selective reduced integration procedures (Hughes, 1987). Brezzi and Fortin (1991) present a detailed analysis of these methods which are encompassed within the general framework of mixed methods, and Arnold (1990) presents a lucid account of mixed finite element methods for elliptic problems. It is well known that low-order, h-version finite elements cause Poisson locking as the incompressible limit is approached ($\nu \rightarrow 0.5$ or $\lambda \rightarrow \infty$). The incompressibility constraint tends to impose far too many constraints in the discrete finite element space, and the trial function space is reduced to nullity leading to the phenomena of mesh locking ($\mathbf{u} \cong 0$). For analytical as well as computational issues related to locking, see Babuška and Suri (1992), Suri (1996), and Chilton and Suri (1997). Mixed methods with displacements and pressure as independent variables, and selective reduced integration procedures have been successful in ameliorating this problem. Malkus and Hughes (1978) have shown the equivalence of mixed finite element methods to selective reduced integration techniques.

The scope and application of meshless methods (Belytschko et al., 1996) in mixed formulations has not been explored to any depth so far. In meshless methods, there is greater flexibility than finite elements in the choice and smoothness (C^k, $k > 0$) of trial function spaces. Donning (1997) used the notion of locking-free interpolants that are based on cardinal splines to solve thin as well as thick beam and plate problems using Mindlin-Reissner theory. By judicious choice of local basis functions in the Partition of Unity Method (PUM) (Melenk and Babuška, 1996), Babuška and Zhang (1998) provided a theoretical basis for removing locking in the thin beam limit.

6.2 Displacement and Pressure Interpolation

We consider the interpolation schemes for the displacements and the presurre in the mixed natural element method. The displacement vectors $\mathbf{u}^h(\mathbf{x}) : \ \Omega \subset \mathbb{R}^2 \to \mathbb{R}^2$ are interpolated using natural neighbor shape functions, and can be written in the form:

$$\mathbf{u}^h(\mathbf{x}) = \sum_{I=1}^{n} \phi_I(\mathbf{x})\mathbf{u}_I, \tag{6.1}$$

where $\mathbf{u}_I$ ($I = 1, 2, \ldots, n$) are the vectors of nodal displacements at the n natural neighbors, and $\phi_I(\mathbf{x})$ are the shape functions associated with each node.
The pressure field is interpolated by an interpolation scheme akin to Eq. (6.1):

$$p^h(\mathbf{x}) = \sum_{I=1}^{n} \psi_I(\mathbf{x})\bar{p}_I, \tag{6.2}$$

where $\psi_I(\mathbf{x})$ is the shape function associated with node I and $\bar{p}_I$ are the nodal pressures. We consider $\psi_I(\mathbf{x})$ to be of the general form

$$\psi_I(\mathbf{x}) = \frac{\big(\phi_I(\mathbf{x})\big)^k}{\sum_J \big(\phi_J(\mathbf{x})\big)^k}, \tag{6.3}$$

where k is a non-negative integer. The case $k = 1$ reduces to natural neighbor interpolation, and all other k render shape functions that form a partition of unity, with the resulting interpolant satisfying only constant completeness. For $k > 1$, numerical studies show that severe Poisson locking results; the cases $k = 0$ and $k = 1$ performed well in the near incompressible limit and hence merit investigation. These two cases are considered for the interpolation of the pressure field, and Eq. (6.2) takes the specific forms:

$$p^h(\mathbf{x}) = \sum_{I=1}^{n} \frac{1}{n} \bar{p}_I, \tag{6.4a}$$

$$p^h(\mathbf{x}) = \sum_{I=1}^{n} \phi_I(\mathbf{x}) \bar{p}_I. \tag{6.4b}$$

The shape functions $\psi_I(\mathbf{x})$ for $k = 0$ that are used to interpolate the pressure need some elaboration. On the basis of Eq. (6.4a) in conjunction with the variation of natural neighbors for a point $\mathbf{x}$, we note that the shape functions $\psi_I(\mathbf{x}) = 1/n$ are C^{-1} with discontinuities along the union of the boundary of support of $\phi_I(\mathbf{x})$ and the intersection of the boundary of support $\partial\Omega_{Jc}$ of all other $\phi_J(\mathbf{x})$ with the domain of support Ω_{Ic} of node I—see Section 3.3.4. The variation of natural neighbors for a regular (5×5) grid is shown in Fig. 3.5. Since the shape function $\psi_I(\mathbf{x}) = 1/n$ is the inverse of the number of natural neighbors for a point $\mathbf{x}$, the above inference is readily observed. An alternate C^{-1} pressure interpolant can be constructed using the well-known concept of nearest neighbors in computational geometry (Preparata and Shamos, 1985). This leads to the interpolation scheme known as nearest neighbor interpolation. In this approach, if $\mathbf{x} \in T_I$, where T_I is the Voronoi polygon of node I, then we assign the nodal pressure $\bar{p}_I$ to $p(\mathbf{x})$. In essence, the pressure field is assumed to be a constant over the Voronoi polygon T_I. In the context of natural neighbor interpolation, if $\phi_I = \|\boldsymbol{\phi}\|_\infty$, then $\psi_I(\mathbf{x}) = 1$ and $\psi_J(\mathbf{x}) = 0 \ \forall\ J \neq I$, and therefore

$$p(\mathbf{x}) = \bar{p}_I \quad \text{if } \mathbf{x} \in T_I. \tag{6.5}$$

6.3 Governing Equations and Mixed Formulation

6.3.1 Strong Form

Consider an open bounded domain $\Omega \subset \mathbb{R}^2$ with boundary Γ. Let $\mathbf{n}$ be the unit normal vector to Γ; the closure of Ω is denoted by $\bar{\Omega} = \Omega \cup \Gamma$. In Section 4.3, the field equations for compressible elasticity, essential and traction boundary conditions, and the principle of virtual work (weak form) are presented. Here, we consider the governing equations for two-dimensional small displacement elastostatics, with validity for both compressible and incompressible material behavior. The presentation closely follows that which is pursued in Section 4.3, and we repeat some of the equations for clarity and completeness. Let the prescribed values of tractions on the traction boundary Γ_t be $\bar{\mathbf{t}}$ and that on the essential boundary Γ_u be $\bar{\mathbf{u}}$ ($\Gamma = \Gamma_u \cup \Gamma_t$). We let $\boldsymbol{\sigma}$ be the Cauchy stress for a kinematically admissible displacement field $\mathbf{u}$, and $\mathbf{b}$ be the body force per unit volume. The strong form for the elastostatic boundary value problem is given by (Hughes, 1987)

$$\text{Given } \mathbf{b} : \Omega \times \Omega \to \mathbb{R}^2, \;\; \bar{\mathbf{u}} : \Gamma_u \times \Gamma_u \to \mathbb{R}^2, \;\; \text{and } \bar{\mathbf{t}} : \Gamma_t \times \Gamma_t \to \mathbb{R}^2$$

$$\text{Find } \mathbf{u} : \bar{\Omega} \times \bar{\Omega} \to \mathbb{R}^2,\ p : \bar{\Omega} \to \mathbb{R} \text{ such that}$$

$$\boldsymbol{\nabla} \cdot \boldsymbol{\sigma} + \mathbf{b} = 0 \quad \text{in } \Omega, \tag{6.6a}$$

$$\boldsymbol{\nabla} \cdot \mathbf{u} + \frac{p}{\lambda} = 0 \quad \text{in } \Omega, \tag{6.6b}$$

$$\mathbf{u} = \bar{\mathbf{u}} \quad \text{on } \Gamma_u, \tag{6.6c}$$

$$\boldsymbol{\sigma} \cdot \mathbf{n} = \bar{\mathbf{t}} \quad \text{on } \Gamma_t, \tag{6.6d}$$

where the Cauchy stress tensor $\boldsymbol{\sigma}$ is related to the small strain tensor $\boldsymbol{\varepsilon}$ and the pressure parameter p (hydrostatic pressure if $\nu = 0.5$) for an isotropic linear elastic material through the constitutive relation:

$$\sigma_{ij} = -p\delta_{ij} + \bar{C}_{ijkl}\varepsilon_{kl}, \tag{6.6e}$$

$$\bar{C}_{ijkl} = \mu(\delta_{ik}\delta_{jl} + \delta_{il}\delta_{jk}). \tag{6.6f}$$

In Eq. (6.6), λ and μ are Lamé parameters which for plane strain are defined as

$$\lambda = \frac{\nu E}{(1+\nu)(1-2\nu)}, \quad \mu = \frac{E}{2(1+\nu)}, \tag{6.7}$$

where ν is the Poisson's ratio. The kinematic relation between the small strain tensor $\boldsymbol{\varepsilon}$ and the displacement vector $\mathbf{u}$ is

$$\boldsymbol{\varepsilon} = \frac{1}{2}\left(\boldsymbol{\nabla}\mathbf{u} + (\boldsymbol{\nabla}\mathbf{u})^T\right). \tag{6.8}$$

6.3.2 Weak Form

We first define the trial and test spaces for the displacements and the pressure. Following Hughes (1987), we let

$$\mathbf{u} \in \mathbf{V} = (H^1(\Omega))^2 \quad \text{(displacement trial solution space)}, \tag{6.9a}$$

$$\mathbf{v} \in \mathbf{V}_0 = (H_0^1(\Omega))^2 \quad \text{(displacement test function space)}, \tag{6.9b}$$

$$p,\, q \in P = L^2(\Omega) \quad \text{(space of pressures—trial and test functions)}, \tag{6.9c}$$

where the Sobolev spaces $H^1(\Omega)$ and $H_0^1(\Omega)$ are defined in Section 2.1.1.

Let $(\mathbf{u}, p) \in \mathbf{V} \times P$ be the trial function pair, and $(\mathbf{v}, q) \in \mathbf{V}_0 \times P$ the corresponding test functions. On taking the product of Eq. (6.6a) with v_i and Eq. (6.6b) with q, and then integrating their sum over the domain Ω, we obtain

$$\underbrace{\int_\Omega \sigma_{ji,j} v_i \, d\Omega + \int_\Omega b_i v_i \, d\Omega}_{(A)} + \int_\Omega \left(u_{k,k} + \frac{p}{\lambda} \right) q \, d\Omega = 0, \tag{6.10}$$

and on using Eq. (4.10) for the integrals marked by (A), we obtain

$$-\int_\Omega \sigma_{ij}(\mathbf{u}) \varepsilon_{ij}(\mathbf{v}) \, d\Omega + \int_\Omega b_i v_i \, d\Omega + \int_{\Gamma_t} \bar{t}_i v_i \, d\Gamma + \int_\Omega u_{k,k} q \, d\Omega + \frac{1}{\lambda} \int_\Omega pq \, d\Omega = 0. \tag{6.11}$$

Now, on using the constitutive equation given in Eqs. (6.6e) and (6.6f), we can write the above equation as

$$\begin{aligned} 2\mu \int_\Omega \varepsilon_{ij}(\mathbf{u}) \varepsilon_{ij}(\mathbf{v}) \, d\Omega - \int_\Omega p v_{k,k} \, d\Omega - \int_\Omega u_{k,k} q \, d\Omega - \frac{1}{\lambda} \int_\Omega pq \, d\Omega \\ = \int_\Omega b_i v_i \, d\Omega + \int_{\Gamma_t} \bar{t}_i v_i \, d\Gamma, \end{aligned} \tag{6.12}$$

and since the test functions v_i and q are independent and arbitrary, we obtain the Hermann variational (weak) form, which is posed as (Hermann, 1965; Hughes, 1987):

Find $(\mathbf{u}, p) \in \mathbf{V} \times P$ such that

$$\bar{a}(\mathbf{u}, \mathbf{v}) + b(\mathbf{v}, p) = \langle \mathbf{b}, \mathbf{v} \rangle + \langle \bar{\mathbf{t}}, \mathbf{v} \rangle \quad \forall \, \mathbf{v} \in \mathbf{V}_0, \tag{6.13a}$$

$$b(\mathbf{u}, q) - \frac{1}{\lambda}(p, q) = 0 \quad \forall \, q \in P, \tag{6.13b}$$

where

$$\bar{a}(\mathbf{u},\mathbf{v}) = 2\mu\int_{\Omega}\varepsilon_{ij}(\mathbf{u})\varepsilon_{ij}(\mathbf{v})\,d\Omega, \tag{6.13c}$$

$$b(\mathbf{v},p) = -\int_{\Omega} p\boldsymbol{\nabla}\cdot\mathbf{v}\,d\Omega. \tag{6.13d}$$

In a displacement-pressure mixed formulation for linear elasticity, the bilinear form $\bar{a}(\mathbf{u},\mathbf{v}) : \mathbf{V}\times\mathbf{V}_0 \to \mathbb{R}$ is symmetric, bounded, and positive definite. Hence, for the displacement-pressure pair $(\mathbf{u},p)$ to be the unique solution to the system in Eq. (6.13), the bilinear form $b(\mathbf{v},p) : \mathbf{V}_0\times P \to \mathbb{R}$ must satisfy the LBB stability condition (Brezzi and Fortin, 1991):

$$\inf_{p\in P}\sup_{\mathbf{v}\in\mathbf{V}_0}\frac{|b(\mathbf{v},p)|}{||\mathbf{v}||_{\mathbf{V}}||p||_P} \geq \beta > 0, \tag{6.14}$$

where β is a constant.

In the numerical implementation, finite-dimensional subspaces are used as the trial and test spaces for the displacements and pressure. Let $\mathbf{V}^h \subset \mathbf{V}$ and $\mathbf{V}_0^h \subset \mathbf{V}_0$ be the trial and test spaces for the displacements, and $P^h \subset P$ be the trial and test space for the pressure. The weak form for NEM can be written as

$$\text{Find } (\mathbf{u}^h,p^h)\in\mathbf{V}^h\times P^h \text{ such that}$$

$$\bar{a}(\mathbf{u}^h,\mathbf{v}^h) + b(\mathbf{v}^h,p^h) = \langle\mathbf{b},\mathbf{v}^h\rangle + \langle\bar{\mathbf{t}},\mathbf{v}^h\rangle \quad \forall\;\mathbf{v}^h\in\mathbf{V}_0^h, \tag{6.15a}$$

$$b(\mathbf{u}^h,q^h) - \frac{1}{\lambda}(p^h,q^h) = 0 \quad \forall\;q^h\in P^h. \tag{6.15b}$$

The LBB stability condition for the discrete problem is similar to Eq. (6.14), with the trial and test functions in the continuous space being replaced by their discrete counterparts.

6.3.3 Discrete System for NEM

Consider the numerical implementation for the mixed natural element method. In a Galerkin procedure, the displacement trial and test functions are interpolated using the same set of shape functions and likewise for the pressure trial and test functions. The trial and test functions are:

$$\mathbf{u}^h(\mathbf{x}) = \sum_{I=1}^{n} \phi_I(\mathbf{x})\mathbf{u}_I, \quad \mathbf{v}^h(\mathbf{x}) = \sum_{I=1}^{n} \phi_I(\mathbf{x})\mathbf{v}_I, \tag{6.16a}$$

$$p^h(\mathbf{x}) = \sum_{I=1}^{n} \psi_I(\mathbf{x})\bar{p}_I, \quad q^h(\mathbf{x}) = \sum_{I=1}^{n} \psi_I(\mathbf{x})\bar{q}_I. \tag{6.16b}$$

The strain-displacement relation for the displacement trial function can be written as

$$\boldsymbol{\varepsilon}^h(\mathbf{x}) = \sum_{I=1}^{n} \mathbf{B}_I\mathbf{u}_I, \tag{6.17}$$

where

$$\mathbf{B}_I = \begin{bmatrix} \phi_{I,1}(\mathbf{x}) & 0 \\ 0 & \phi_{I,2}(\mathbf{x}) \\ \phi_{I,2}(\mathbf{x}) & \phi_{I,1}(\mathbf{x}) \end{bmatrix}. \tag{6.18}$$

The divergence of the displacement trial solution is given by

$$\boldsymbol{\nabla} \cdot \mathbf{u}^h(\mathbf{x}) = \sum_{I=1}^{n} \tilde{\mathbf{B}}_I \mathbf{u}_I, \tag{6.19}$$

where

$$\tilde{\mathbf{B}}_I = \begin{bmatrix} \phi_{I,1}(\mathbf{x}) & \phi_{I,2}(\mathbf{x}) \end{bmatrix}. \tag{6.20}$$

On substituting the displacement and pressure trial and test functions in Eq. (6.15) and using the arbitrariness of displacement and pressure nodal variations, the following discrete system of linear equations is obtained (Hughes, 1987):

$$\begin{bmatrix} \bar{\mathbf{K}} & \mathbf{G} \\ \mathbf{G}^T & \mathbf{M} \end{bmatrix} \begin{Bmatrix} \mathbf{d} \\ \mathbf{p} \end{Bmatrix} = \begin{Bmatrix} \mathbf{f} \\ \mathbf{0} \end{Bmatrix}, \tag{6.21}$$

where

$$\bar{\mathbf{K}}_{IJ} = \int_{\Omega^h} \mathbf{B}_I^T \bar{\mathbf{C}} \mathbf{B}_J \, d\Omega, \tag{6.22a}$$

$$\mathbf{G}_{IJ} = -\int_{\Omega^h} \tilde{\mathbf{B}}_I^T \psi_J \, d\Omega, \tag{6.22b}$$

$$\mathbf{M}_{IJ} = -\frac{1}{\lambda} \int_{\Omega^h} \psi_I \psi_J \, d\Omega, \tag{6.22c}$$

$$\mathbf{f}_I = \int_{\Omega^h} \phi_I \mathbf{f} \, d\Omega + \int_{\Gamma_t^h} \phi_I \bar{\mathbf{t}} \, d\Gamma. \tag{6.22d}$$

In the above equations, $\mathbf{d}$ is the vector of nodal displacements and $\mathbf{p}$ is the vector of nodal pressures. The matrix $\bar{\mathbf{K}}$ is symmetric and positive definite, and the matrix $\mathbf{M}$ is symmetric and negative definite ($\mathbf{M} = \mathbf{0}$ when $\nu = 0.5$). The matrix $\mathbf{G}$ corresponds to the discrete gradient operator, and $\mathbf{G}^T$ to the discrete divergence operator.

6.4 Numerical Results and Discussions

The application of the mixed natural element method to problems in small displacement compressible as well as near incompressible two-dimensional elastostatics, in the absence of body forces, is presented. In the computations, numerical integration is carried out using symmetric quadrature rules for a triangle (Dunavant, 1985). Three point quadrature rule is used in the numerical integration of the weak form; the error norm computations are carried out using 25 point quadrature rule in each triangle.

6.4.1 Cantilever Beam

In Fig. 4.10, a cantilever beam subjected to a parabolic end load is illustrated. The beam has length L, height D, and unit thickness. The problem description and illustration for this problem are given in Section 4.4.4. The displacement vector solution and the exact stresses are given in Eqs. (4.28) and (4.30). In the numerical model, the analytical displacement solution from Eq. (4.28) is prescribed on the boundary Γ_u: $x_1 = 0$, $-D/2 \leq x_2 \leq D/2$ (Fig. 4.10). On the remaining boundaries, exact tractions are specified. The following parameters are used in the numerical computations: $P = -1000$ lb, $D = 1$ in., $L = 4$ in., $E = 3 \times 10^7$ psi, and plane strain conditions are assumed.

The mixed natural element displacement-pressure formulation is applied to both the compressible and near incompressible cases. The numerical computations are carried out using four different nodal discretizations, namely 85 nodes, 297 nodes, 1105 nodes, and 1701 nodes. Equal nodal spacing in the x_1- and x_2-direction is used in each of the above grids. A sample nodal discretization (85 nodes) is shown in Fig. 4.11. In Table 6.1, the normalized end displacement $\big(u_2^h(4,0)/u_2(4,0)\big)$ is presented for varying Poisson's ratio using FEM, C^0 NEM, and the mixed formulation. The results presented in Table 6.1 are for the nodal discretization shown in Fig. 4.11. Bilinear quadrilateral elements with 3×3 Gauss quadrature are used in the finite element computations, and three point symmetric quadrature rule over triangles is used in the NEM computations. Clearly, severe locking is observed for both, FEM and NEM as $\nu \to 0.5$; the mixed C^0–C^0 method does lock to some degree, but the mixed C^0–C^{-1} method does seem to alleviate locking as the incompressible limit is approached. The results for the mixed C^0–C^{-1} formulation are accurate for the entire range of values of ν.

A convergence study for the cantilever beam problem is carried out. We define the $L^2(\Omega)$ and energy error norms used in the analysis as:

$$\|\mathbf{u}-\mathbf{u}^h\|_{L^2(\Omega)} = \Big(\big(\mathbf{u}-\mathbf{u}^h, \mathbf{u}-\mathbf{u}^h\big)\Big)^{1/2}, \tag{6.23a}$$

$$\|\mathbf{u}-\mathbf{u}^h\|_{E(\Omega)} = \left(\frac{1}{2}a\big(\mathbf{u}-\mathbf{u}^h, \mathbf{u}-\mathbf{u}^h\big)\right)^{1/2}, \tag{6.23b}$$

where

$$a(\mathbf{u},\mathbf{u}) = 2\mu\big(\boldsymbol{\varepsilon}(\mathbf{u}), \boldsymbol{\varepsilon}(\mathbf{u})\big) + (p, \mathrm{div}\ \mathbf{u}). \tag{6.23c}$$

In Figures 6.1 and 6.2, the relative displacement and energy error norms are plotted against the nodal spacing h on a log-log plot. Results are presented for the mixed

Table 6.1: Normalized end displacement for the cantilever beam problem.

ν	FEM (3×3)	NEM		
		C^0	Mixed $(C^0$–$C^0)$	Mixed $(C^0$–$C^{-1})$
0.3	0.9651	0.9692	0.9739	0.9903
0.4	0.9373	0.9436	0.9676	0.9924
0.4999	0.1873	0.1950	0.9495	0.9901
0.4999999	0.1775	0.2103	0.9490	0.9903

C^0–C^0 displacement-pressure and C^0–C^{-1} displacement-pressure formulations. The error norm computations are carried out for three different values of the Poisson's ratio: $\nu = 0.3$, $\nu = 0.4$, and $\nu = 0.4999$ (near incompressibility). The rate of convergence is denoted by the value of R. The results indicate that optimal convergence in displacement and energy is attained for all three values of ν. The absolute accuracy of the C^0–C^{-1} formulation is better than that obtained for the C^0–C^0 formulation.

The pressure computations are carried out along the mid-section of the beam using the mixed C^0–C^0 and C^0–C^{-1} methods. The results are computed at 100 equi-distant points between $y = -0.5$ in. and $y = 0.5$ in. In Fig. 6.3, the variation of the pressure parameter p for the 85 node grid is shown for the compressible case ($\nu = 0.3$). The

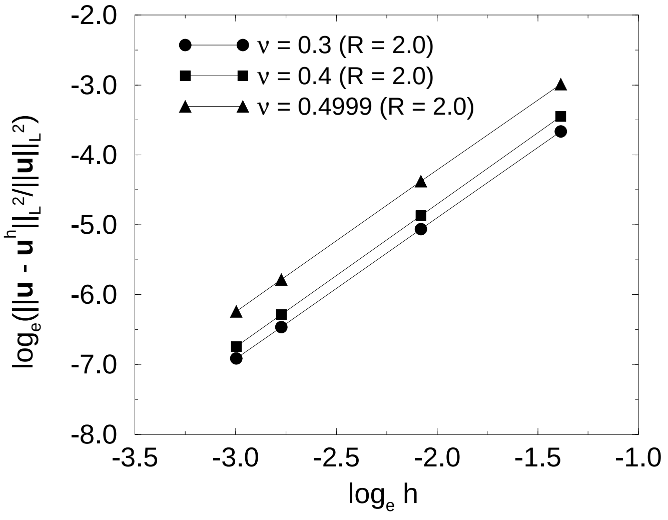

(a)

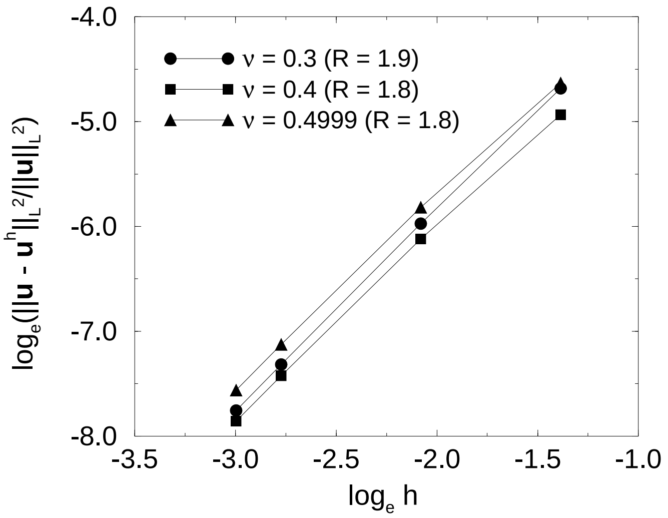

(b)

Figure 6.1: Rate of convergence in displacement for the cantilever beam problem. (a) C^0–C^0 method, and (b) C^0–C^{-1} method.

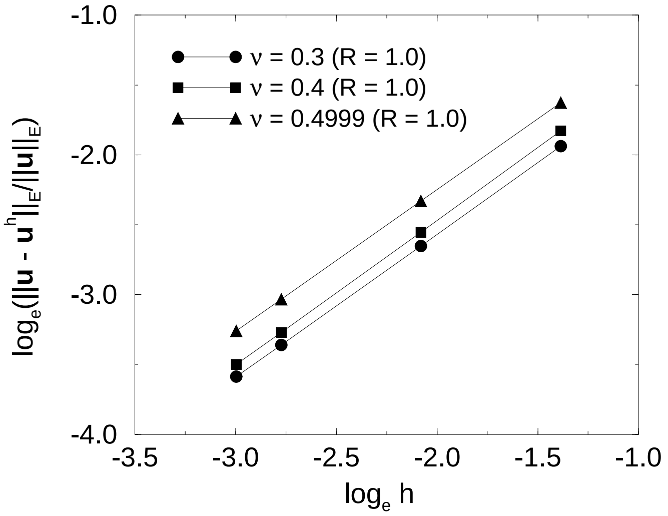

(a)

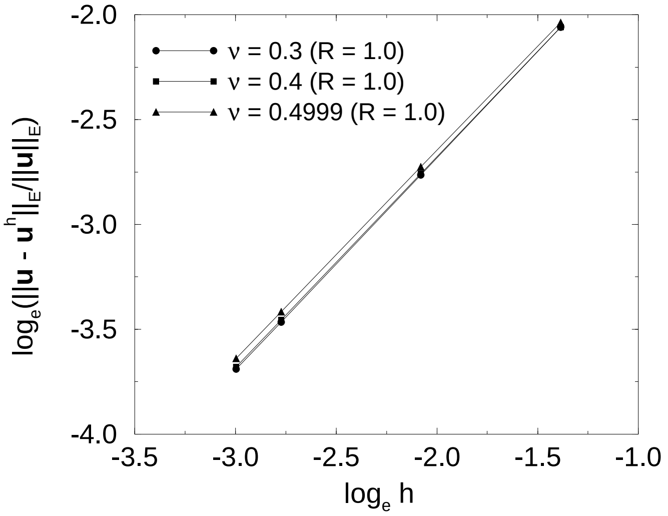

(b)

Figure 6.2: Rate of convergence in energy for the cantilever beam problem. (a) C^0–C^0 method, and (b) C^0–C^{-1} method.

pressure parameter p is given by

$$p = \frac{-\sigma_{kk} + 2\mu\varepsilon_{kk}}{3}, \tag{6.24}$$

and hence in the incompresssible limit (div $\mathbf{u} = \varepsilon_{kk} = 0$), p is the hydrostatic pressure. In Fig. 6.4, the hydrostatic pressure is plotted for the near incompressible case (85 and 1701 nodal grids). The pressure oscillation for the C^0–C^0 method are fairly pronounced, while the results for the C^0–C^{-1} method are less oscillatory.

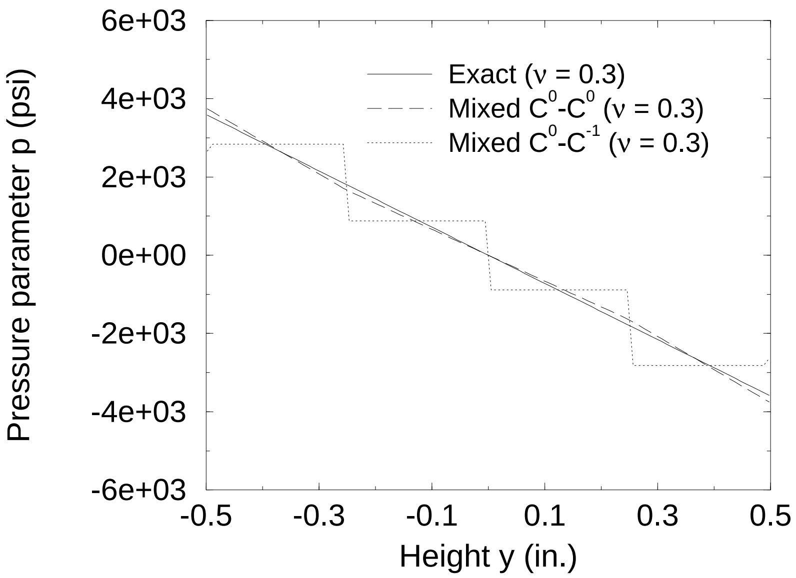

Figure 6.3: Variation of the pressure parameter p for the beam model.

6.4.2 Infinite Plate with a Circular Hole

In order to test the accuracy of the mixed formulation in near incompressible elasticity, it is imperative that we also study its performance for non-uniform nodal discretiza-

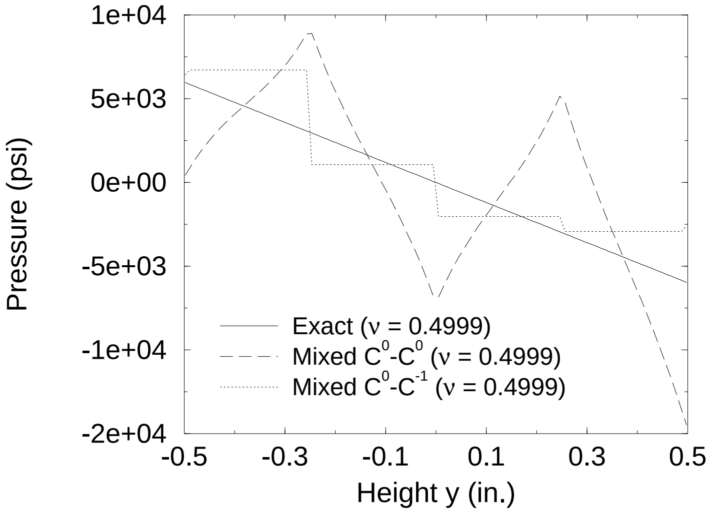

(a)

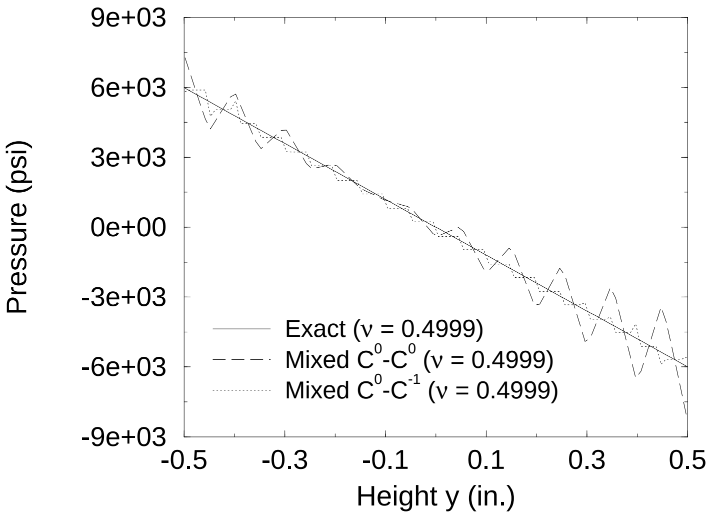

(b)

Figure 6.4: Variation of hydrostatic pressure for the beam model. (a) 85 nodes, and (b) 1701 nodes.

tions. We consider the problem of an infinite plate with a traction free circular hole under unidirectional tension along the x_1-direction (Fig. 4.6). The illustration of the model problem, with a description of the essential and traction boundary conditions is discussed in Section 4.4.3. The exact stress solution is given in Eq. (4.25) and the exact displacement components are presented in Eq. (4.26).

In the numerical computations, $a = 1$ in., $L = 5$ in., and plane strain conditions are assumed. The mixed natural element displacement-pressure formulation is applied to both the compressible and near incompressible cases. A convergence study is carried out using four different nodal discretizations (Fig. 4.7). The $L^2(\Omega)$ and energy error norms used in the computations are defined in Eq. (6.23). In Figures 6.5 and 6.6, the relative displacement and energy error norms are plotted against the square root of the number of nodes on a log-log plot. Results are presented for the mixed C^0–C^0 displacement-pressure and C^0–C^{-1} displacement-pressure formulations. The error norm computations are carried out for three different values of the Poisson's ratio: $\nu = 0.3$, $\nu = 0.4$, and $\nu = 0.4999$ (near incompressibility). The convergence rates which are denoted by R are indicated on the plots. The results indicate that near optimal convergence in displacement and energy is attained for all three values of ν. The absolute accuracy of the C^0–C^{-1} formulation is better than that obtained for the C^0–C^0 formulation; the relative error norms using the mixed C^0–C^{-1} method are independent of the Poisson's ratio ν.

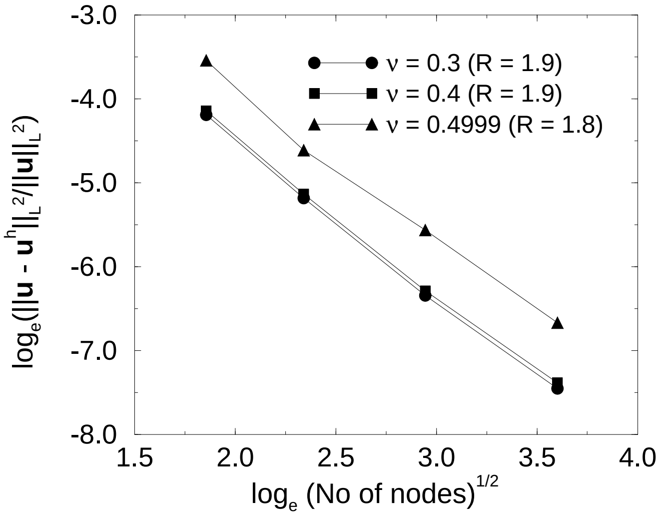

(a)

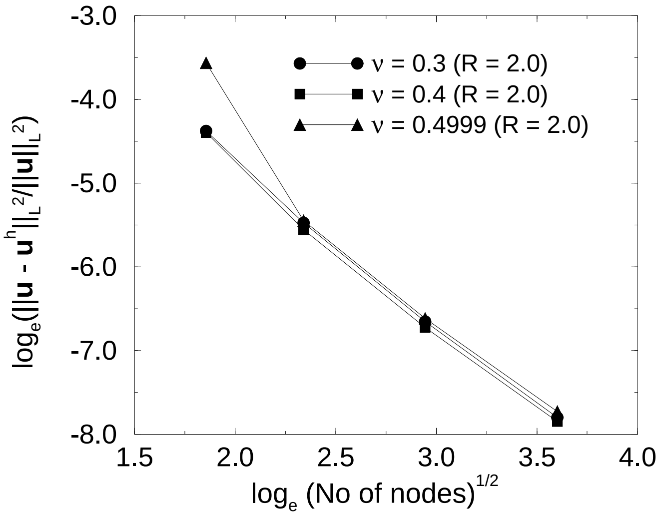

(b)

Figure 6.5: Rate of convergence in displacement for the plate with a hole problem. (a) C^0–C^0 method, and (b) C^0–C^{-1} method.

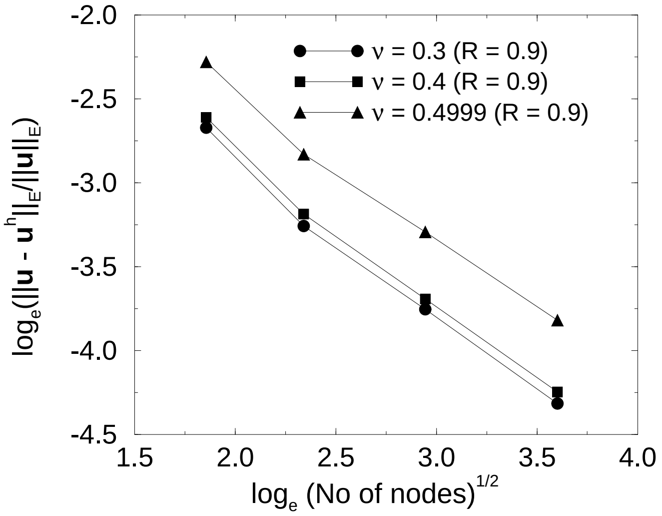

(a)

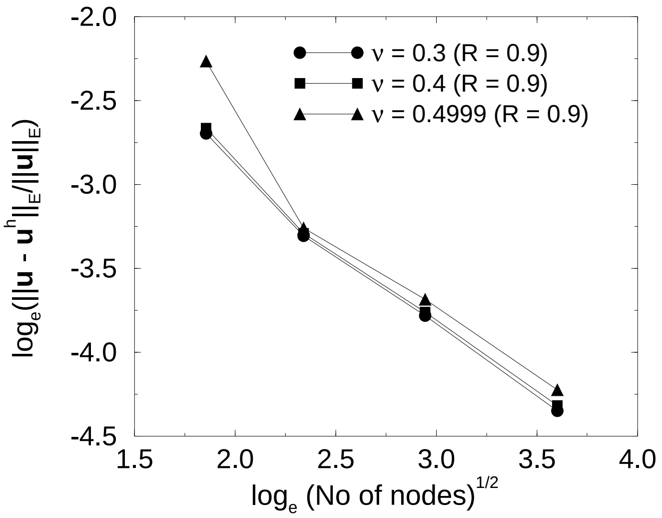

(b)

Figure 6.6: Rate of convergence in energy for the plate with a hole problem. (a) C^0–C^0 method, and (b) C^0–C^{-1} method.